

Rearrangements of Water Dimer and Hexamer

David J. Wales

University Chemical Laboratories, Lensfield Road, Cambridge, CB2 1EW, United Kingdom

Abstract. Rearrangement mechanisms of the water dimer and the cage form of the water hexamer are examined theoretically with particular reference to tunneling splittings and spectroscopy. The three lowest barrier rearrangements of the water dimer are characterized by *ab initio* methods and compared with the results of previous constrained calculations. The acceptor-tunneling pathway does not proceed via a direct rotation around the C_2 axis of the acceptor, but rather via relatively asynchronous rotation of the donor about the hydrogen bond and an associated ‘wag’ of the acceptor. Rearrangements between different cage isomers of the water hexamer are studied for two empirical potentials. The experimentally observed triplet splittings may be the result of flip and bifurcation rearrangements of the two single-donor, single-acceptor monomers. Two-dimensional quantum calculations of the nuclear dynamics suggest that delocalization over more than one cage isomer may occur, especially in excited states.

This paper was written in October 1996 for *Theory of Atomic and Molecular Clusters* edited by Julius Jellinek, which has unfortunately still failed to appear.

1 Introduction

Water clusters have proved to be attractive systems for study to both theory and experiment, particularly in the last two decades. This popularity may be ascribed in part to the role of water as an almost universal solvent in chemistry and biochemistry, but also to the importance of developing a fundamental understanding of intermolecular forces [1-4]. A recent flurry of activity has been sparked by the advent of far-infrared vibration-rotation tunneling (FIR-VRT) spectroscopy [5-8], where resolutions of up to 1 MHz have been achieved. These results provide a new challenge to theory because the tunneling splittings that can now be resolved necessitate a global view of the potential energy surface (PES) if they are to be explained. The large amplitude motions which are typical of such weakly bound Van der Waals complexes sample regions of the PES that are far removed from the bottom of potential wells, and provide new information about the nature of the intermolecular forces. Furthermore, to explain or predict the tunneling splittings theory must characterize not only minima but transition states and rearrangement mechanisms.

The interplay between theory and experiment is perhaps best illustrated by our recently improved understanding of the dynamics exhibited by water trimer, which began with the FIR-VRT experiment of Pugliano and Saykally [9]. These authors reported spectra for $(\text{D}_2\text{O})_3$ characteristic of an oblate symmetric rotor, with each line split into a regularly spaced quartet and a spacing of roughly 6 MHz, i.e. $2 \times 10^{-4} \text{ cm}^{-1}$. Accurate values for the vibrationally averaged rotational constants revealed a large negative inertial defect, indicative of extensive out-of-plane motion of the non-hydrogen-bonded hydrogens. However, a cyclic, asymmetric global minimum structure for the trimer was established some years ago in *ab initio* calculations [10], in agreement with earlier experimental results [11].

The oblate symmetric top spectrum of the trimer has now been explained by vibrational averaging over large amplitude torsional motions of the free hydrogens on the timescale of the FIR-VRT experiment. These large amplitude motions are associated with a facile ‘flip’ rearrangement where a free hydrogen moves from one side of the plane defined by the three oxygen atoms to the other. This mechanism was probably first characterized for an empirical potential by Owicki *et al.* [12]. An *ab initio* pathway has been presented by Wales [13] and the corresponding transition state was also characterized by Fowler and Schaefer [14]. Wales identified two other degenerate rearrangement mechanisms for the trimer with rather larger barriers than the flip, and suggested that one of them (christened the ‘donor’ or ‘bifurcation’ pathway) might be responsible for the quartet splittings observed experimentally [13]. In the associated transition state one monomer acts as a double donor to a neighbour which acts as a double acceptor in a configuration similar to that of the ‘donor tunneling’ transition state in the water dimer, discussed in §4.

Subsequent experiments [15-16] assigned new transitions for $(\text{H}_2\text{O})_3$ and $(\text{D}_2\text{O})_3$ which revealed rigorously symmetric rotor structure, in contrast to the strongly perturbed band that was initially investigated by Pugliano and Saykally [9]. All the transitions reported by Liu *et al.* [15] and Suzuki and Blake [16] show a regular quartet splitting of every rovibrational transition. Liu *et al.* reported that their new spectra were consistent with the $G(48)$ group suggested by the mechanisms discovered by Wales [13]. Walsh and Wales have recently studied the bifurcation mechanism in more detail and discovered that six slightly different alternatives exist, depending upon the level of the calculation employed [17].

Numerous other treatments of the water trimer have focused on the breakdown of the total energy into many-body contributions and the effects of electron correlation [18-22], the development of torsional potential energy surfaces [23-25], the calculation of torsional energy levels using the discrete variable representation (DVR) [26-29] and quantum simulations of the nuclear dynamics using the diffusion Monte Carlo (DMC) method [30-31].

In the present contribution we report new results for the water dimer and water hexamer, which lie at the two limits of the size range for which high resolution data have been obtained. Unconstrained pathways do not seem to have been described before for the three rearrangements of the water dimer

which lead to observable splittings or shifts in the pattern of rovibrational energy levels. In particular, we find that the acceptor tunneling mechanism is not simply a rotation about the local C_2 axis of the acceptor monomer. For water hexamer we employ two empirical intermolecular potentials to examine the cage isomers and show that these structures are connected by facile, non-degenerate single flips of the two single-donor, single-acceptor monomers. Two-dimensional DVR calculations are performed to investigate these motions. First we give a brief overview of the effective molecular symmetry group which must be employed to classify the energy levels of floppy molecules.

2 The Effective Molecular Symmetry Group

The observation of quantum tunneling effects in high resolution spectra provides indirect information about the corresponding rearrangement mechanisms. To make use of this information we need to employ group theory to classify the energy levels of such systems. Point groups prove satisfactory when the molecule under consideration is rigid on the appropriate experimental timescale. However, molecular potential energy surfaces generally contain local minima corresponding to permutational isomers of any given stationary point. We will adopt the nomenclature of Bone *et al.* [32] where a ‘structure’ is understood to mean a particular molecular geometry and a ‘version’ is a particular labelled permutational isomer of a given structure. Minima which are directly connected by a given rearrangement are said to be ‘adjacent’.

Tunneling splittings may be observed when rovibronic wavefunctions localized in the potential wells corresponding to different versions interfere with each other. For example, the ammonia molecule displays doublet splittings because pairs of permutational isomers are interconverted by the inversion mechanism in which the molecule passes through a planar transition state [33-34]. If the barrier corresponding to a certain rearrangement mechanism is sufficiently low, the path length sufficiently short, and the associated effective mass sufficiently small then tunneling may occur. Hence tunneling splittings can usually be associated with a low energy transition state corresponding to a degenerate rearrangement mechanism [35] which links different versions of the same structure, as opposed to different structures where the energy levels would not be in resonance. Degenerate rearrangements can be either symmetric or asymmetric, depending upon whether the two sides of the corresponding path are related by symmetry [36]. We follow Murrell and Laidler’s definition of a transition state as a stationary point with a single negative Hessian eigenvalue [37].

The energy levels of non-rigid molecules can be classified using the Complete Nuclear Permutation-Inversion (CNPI) group which is the direct product of the group containing all possible permutations of identical nuclei and the inversion group. The latter group contains only the identity operation, E , and the operation of inversion of all particle coordinates through the space-fixed origin, E^* , which commutes with all the permutations. The CNPI group is a true symmetry group of the full molecular Hamiltonian in the absence of external fields,

and its elements are generally referred to as permutation-inversion operations. However, the order of this group increases factorially for systems containing increasing numbers of atoms of the same element, and rapidly becomes difficult to use. Fortunately, Longuet-Higgins showed that it not necessary to consider the whole of the CNPI group, but rather only the permutation-inversions which correspond to tunneling splittings that are resolvable for a given experiment [38]. The corresponding rearrangement mechanisms are said to be ‘feasible’. The resulting subgroup of the CNPI group is known as the effective molecular symmetry (MS) group. For rigid molecules the appropriate MS group is isomorphic to the usual rigid molecule point group [39-42]. The corresponding permutation-inversions simply correspond to overall rotation of the system, and are therefore always feasible.

If there exists a non-trivial feasible rearrangement with a finite barrier then the MS group is enlarged and the wavefunctions which transform according to irreducible representations of this group are linear combinations of the functions localized in each well. In general, a given mechanism will not link all the possible versions of a given structure but rather the versions will be partitioned into a number of closed sets with equivalent reaction graphs for each set. If we consider a representative set of versions all of which can be interconverted by repeated application of the feasible rearrangement, then the corresponding wavefunction must be a linear combination of the localized functions from members of this set. The delocalized wavefunctions can be found by solving a secular problem, just as in the linear combination of molecular orbitals approach to electronic structure. If the wavefunctions decay rapidly in the classically forbidden regions of the PES between minima then it may be sufficient to consider only nearest-neighbour interactions and the resulting splitting pattern is then determined largely by symmetry. The connectivity of the reaction graph, the associated MS group and the splitting pattern can all be found automatically by a computer program once a minimal set of generator permutation-inversions is known [43].

3 Geometry Optimizations and Potentials

The geometry optimizations and calculations of rearrangement pathways described in the following sections were all performed by eigenvector-following [44]. Details of the precise implementation have been given elsewhere [45-46]. Analytic first and second derivatives of the energy were calculated at every step. In the *ab initio* calculations these derivatives were all generated by the CADPAC program [47], and Cartesian coordinates were used throughout. Pathways were calculated by taking small displacements of $0.03 a_0$ away from a transition state both parallel and antiparallel to the transition vector, and then employing eigenvector-following energy minimization to find the associated minimum. The pathways obtained by this procedure have been compared to steepest-descent paths and pathways that incorporate a kinetic metric [48] in previous work—the mechanism is generally found to be represented correctly [17].

Calculations employing rigid body intermolecular potentials were performed using the ORIENT3 program [49-51], which contains the same optimization package adapted for centre-of-mass/orientational coordinates. This program can treat intermolecular potentials based upon Stone’s distributed multipoles [52-53] and distributed polarizabilities [54-55]; simpler models based upon point charges and Lennard-Jones interactions fall within this framework. Calculations for the water hexamer in §5 were performed using the relatively sophisticated ASP-W2 potential of Millot and Stone [56] (somewhat modified from the published version) and the much simpler but widely-used TIP4P form [57-58].

In the *ab initio* Hartree-Fock (HF) calculations for $(\text{H}_2\text{O})_2$ two basis sets were considered. The smaller double- ζ [59-60] plus polarization (DZP) basis employed polarization functions consisting of a single set of p functions on each hydrogen atom (exponent 1.0) and a set of six d functions on each oxygen atom (exponent 0.9) to give a total of 26 basis functions per monomer. The larger basis set, denoted DZP+diff, includes the above DZP functions with an additional diffuse s function on each hydrogen atom (exponent 0.0441) and diffuse sets of s and p functions on each oxygen atom (exponents 0.0823 and 0.0651 for s and p respectively) [14], to give 32 basis functions per monomer. Correlation corrections were obtained through both second order Møller-Plesset (MP2) theory [61] and density functional theory (DFT). In the DFT calculations we employed the Becke nonlocal exchange functional [62] and the Lee-Yang-Parr correlation functional [63] (together referred to as BLYP); derivatives of the grid weights were not included and the core electrons were not frozen. Numerical integration of the BLYP functionals was performed using grids between the CADPAC ‘MEDIUM’ and ‘HIGH’ options. The ‘MEDIUM’ grids were not accurate enough to give the right number of negative Hessian eigenvalues, whereas the ‘HIGH’ grids contained more points than necessary. CADPAC actually uses different sized grids for different parts of the calculation [47]; in the present work these grids contained 14,386 and 97,008 points after removal of those with densities below the preset tolerances. Calculations were deemed to be converged when the root-mean-square gradient fell below 10^{-6} atomic units. This is sufficient to reduce the six ‘zero’ normal mode frequencies to less than 1 cm^{-1} in the HF and MP2 calculations. Because derivatives of the grid weights were not included, the largest of the six ‘zeros’ can be as big as 20 cm^{-1} for the DFT stationary points.

Three additional parameters are useful in describing the rearrangement mechanisms. The first is the integrated path length, S , which was calculated as a sum over eigenvector-following steps. The second is the distance between the two minima in nuclear configuration space, D . The third is the moment ratio of displacement [64], γ , which gives a measure of the cooperativity of the rearrangement:

$$\gamma = \frac{N \sum_i [\mathbf{Q}_i(s) - \mathbf{Q}_i(t)]^4}{\left(\sum_i [\mathbf{Q}_i(s) - \mathbf{Q}_i(t)]^2 \right)^2}, \quad (1)$$

where $\mathbf{Q}_i(s)$ is the position vector in Cartesian coordinates for atom i in minimum s , etc., and N is the number of atoms. If every atom undergoes the same

displacement in one Cartesian component then $\gamma = 1$, while if only one atom has one non-zero component then $\gamma = N$, i.e. 18 for $(\text{H}_2\text{O})_6$.

4 Rearrangements of Water Dimer

There have been many experimental investigations of the water dimer [65] following the original work of Dyke, Mack and Muentner [66]. Most recently, a complete characterization of the tunneling dynamics in a vibrationally excited state of $(\text{D}_2\text{O})_2$ has been presented [67]. The dimer rovibronic energy levels were first classified in terms of permutation-inversion group theory by Dyke [68], and Coudert and Hougen applied their internal axis approach to the intermolecular dynamics using an empirical potential [69-71]. Smith *et al.* [72] performed *ab initio* calculations and identified three true transition states for $(\text{H}_2\text{O})_2$; they also performed constrained calculations of the donor-tunneling pathway. In this section we will describe unconstrained pathway calculations for all three rearrangements; the energetics of the various stationary points at different levels of theory are summarized in Table 1 and counterpoise-corrected [73] binding energies (including monomer relaxation [74]) are given in Table 2.

There are a total of $2 \times 2! \times 4!/2 = 48$ distinct versions of the water dimer global minimum on the PES (we divide by two because the rigid molecule point group has order two [32]). However, mechanisms which involve the making and breaking of covalent bonds lie much too high in energy to give rise to observable tunneling splittings. The largest possible MS group which can pertain when covalent bond-breaking is not feasible has order $2 \times 2! \times (2!)^2 = 16$, where the first factor accounts for the inversion mechanism, the second factor accounts for permutation of the two oxygen nuclei, and the last term accounts for the permutation of the two hydrogen (or deuterium) atoms within each monomer. This group may be denoted $G(16)$ and is isomorphic to the point group D_{4h} [68]. Since the equilibrium geometry has C_s symmetry the maximum number of distinct versions that can be interconverted without breaking covalent bonds is $16/2 = 8$.

Table 1. Energies in hartree and point groups at various levels of theory for the water dimer global minimum and the transition states for acceptor tunneling, donor-acceptor interchange and donor tunneling.

	DZP/HF	DZP+diff/HF	DZP+diff/BLYP	DZP+diff/MP2
minimum	-152.102057(C_s)	-152.107971(C_s)	-152.87817(C_s)	-152.540770(C_s)
acceptor	-152.101274(C_s)	-152.107282(C_s)	-152.87701(C_1)	-152.539673(C_1)
don-acc	-152.100688(C_i)	-152.106287(C_i)	-152.87591(C_i)	-152.538743(C_i)
donor	-152.099832(C_{2v})	-152.105946(C_{2v})	-152.87535(C_{2v})	-152.538149(C_{2v})

Fig. 1. Acceptor-tunneling path for $(\text{H}_2\text{O})_2$ calculated at the DZP+diff/BLYP level. For this path $S = 4.2 a_0$, $D = 2.8 a_0$ and $\gamma = 1.3$ (see §3).

Fig. 3. Donor-tunneling path for $(\text{H}_2\text{O})_2$ calculated at the DZP+diff/BLYP level. For this path $S = 5.8 a_0$, $D = 4.5 a_0$ and $\gamma = 2.2$ (see §3).

In the equilibrium C_s geometry one ‘donor’ monomer acts as a single hydrogen-bond donor to the other ‘acceptor’ molecule [75]. The largest tunneling splitting is due to a mechanism in which the two hydrogen atoms of the acceptor monomer are effectively interchanged, for which Smith *et al.* [72] reported a barrier of 206 cm^{-1} . In the present work a planar transition state of C_s symmetry was found for both basis sets in the HF calculations, but this changed to an out-of-plane C_1 structure when correlation corrections were applied, in agreement

with Smith *et al.* [72]. The pathway is shown in Fig. 1, and corresponds to a ‘methylamine-type’ process [76] rather than a direct rotation about the local C_2 axis of the acceptor monomer. The path is represented by nine snapshots where the first and last frames are the two minima, the middle frame is the transition state and three additional frames on each side of the path were selected to best illustrate the mechanism. All the pathways in the present work were visualized using Mathematica [77].

The above mechanism is in agreement with the analysis of Pugliano *et al.* [67] for the ground state acceptor tunneling path. The generator permutation-inversion corresponding to the labelling scheme of Fig. 1 is (34), and it connects the versions in pairs. Hence each rigid-dimer rovibrational level is split into two by this process. Experimentally the ground state splitting due to acceptor tunneling is [78] 2.47 cm^{-1} , in good agreement with a five-dimensional treatment of the nuclear dynamics by Althorpe and Clary [79], which yielded a value of 2.34 cm^{-1} . The MS group for the rigid dimer labelled according to Fig. 1 contains only the identity, E , and the permutation-inversion (34)*, where hydrogens three and four change places and all coordinates are inverted through the space-fixed origin. The appropriate MS group when the generator (34) operation is feasible contains the elements E , E^* , (34) and (34)*.

Table 2. Couterpoise-corrected [73] binding energies in millihartree at various levels of theory for the water dimer global minimum and the transition states for acceptor tunneling, donor-acceptor interchange and donor tunneling.

	DZP/HF	DZP+diff/HF	DZP+diff/BLYP	DZP+diff/MP2
minimum	7.42	6.92	7.75	7.45
acceptor	6.88	6.38	6.64	6.65
don-acc	5.73	5.82	6.03	6.52
donor	5.13	5.07	4.79	5.28

The next largest splitting is caused by donor-acceptor interchange. For this process Smith *et al.* [72] found a cyclic transition state with C_i symmetry and an associated barrier of 304 cm^{-1} . In this rearrangement, for which the calculated pathway is shown in Fig. 2, the roles of the donor and acceptor monomers are interchanged. An appropriate generator for the labelling scheme of Fig. 2 is (AB)(1423), i.e. oxygen A is replaced by oxygen B, hydrogen 1 is replaced by hydrogen 4, hydrogen 4 is replaced by hydrogen 2 etc. This generator is not unique—one could also choose (AB)(14)(23)* and obtain the same MS group.

If donor-acceptor interchange is the only feasible mechanism then the versions are connected in sets of four and the MS group has eight members: class 1 contains E , class 2 contains (12)(34), class 3 contains (AB)(1423) and (AB)(1324), class 4 contains (34)* and (12)*, and class 5 contains (AB)(14)(23)*

Fig. 4. Energy versus the integrated path length, S , for the three degenerate rearrangement mechanisms of the water dimer described in §4.

and (AB)(13)(24)*. The splitting pattern in the simplest Hückel-type approximation [80] is:

$$2\beta_{\text{da}}(A_1), \quad 0(E), \quad -2\beta_{\text{da}}(B_1), \quad (2)$$

where β_{da} is the donor-acceptor-interchange tunneling matrix element and we have labelled the levels according to appropriate irreducible representations of the $G(8)$ group which is a subgroup of $G(16)$ [68]. When this process and acceptor tunneling are both feasible the MS group has order 16, i.e. the largest MS group possible without breaking covalent bonds, and is isomorphic to D_{4h} [68]. The versions are then connected in sets of eight and the splitting pattern is:

$$\begin{aligned} \beta_{\text{a}} + 2\beta_{\text{da}}(A_1^+), & \quad \beta_{\text{a}}(E^+), & \quad \beta_{\text{a}} - 2\beta_{\text{da}}(B_1^+), \\ -\beta_{\text{a}} + 2\beta_{\text{da}}(A_2^-), & \quad -\beta_{\text{a}}(E^-), & \quad -\beta_{\text{a}} - 2\beta_{\text{da}}(B_2^-), \end{aligned} \quad (3)$$

where β_{a} is the acceptor-tunneling matrix element. Experimentally, the tunneling splittings due to donor-acceptor-interchange are about a factor of five smaller than those associated with acceptor tunneling.

The third process which is generally presumed to have an observable effect on the energy level diagram is donor tunneling, but this can only lead to energy

level shifts rather than further splittings because $G(16)$ is the largest MS group possible without breaking covalent bonds. Smith *et al.* [72] calculated a barrier of 658 cm^{-1} for this mechanism, and the corresponding pathway found in the present work is shown in Fig. 3. An appropriate generator permutation-inversion for the labelling scheme of Fig. 3 is (12)(34), and on its own this process would simply lead to doublet splittings with versions linked in pairs and an MS group of order 4. However, when combined with the other two mechanisms the eigenvalues of the corresponding secular problem (assuming a Hückel-type approximation [80]) are:

$$\begin{aligned} & \beta_a + 2\beta_{da} + \beta_d(A_1^+), & \beta_a - \beta_d(E^+), & \beta_a - 2\beta_{da} + \beta_d(B_1^+), \\ & -\beta_a + 2\beta_{da} + \beta_d(A_2^-), & -\beta_a - \beta_d(E^-), & -\beta_a - 2\beta_{da} + \beta_d(B_2^-). \end{aligned} \quad (4)$$

This pattern is in complete agreement with that obtained by Althorpe and Clary [79] and with the model calculations of Coudert and Hougen [69-71]. Since the tunneling levels are no longer in plus-minus pairs we conclude that the presence of donor tunneling introduces odd-membered rings into the reaction graph [81].

The DZP+diff/BLYP energy profiles for all three rearrangements are shown in Fig. 4. A maximum step size of $0.1 a_0$ was used for the left-hand side of the acceptor-tunneling path. This value was increased to $0.15 a_0$ for all the other paths, resulting in slightly less smooth profiles but much faster execution time.

5 Water Hexamer

Liu *et al.* [82] have recently identified a VRT band of $(\text{H}_2\text{O})_6$ at 83 cm^{-1} on the basis of an isotope mixture test. In contrast to smaller water clusters the lowest energy isomer of the hexamer is probably not cyclic, and the four lowest energy structures found by Tsai and Jordan [83] lie within an energy range of only 100 cm^{-1} . The most accurate calculations conducted so far suggest that a ‘cage’ structure lies lowest, followed closely by ‘prism’ and ‘book’ forms (Fig. 5) [84]. DMC calculations were used to find the vibrationally averaged rotational constants for each structure using an empirical potential, and the best match was found for the cage structure. On this basis the spectrum was assigned to the cage [82].

There are several unanswered questions concerning the interpretation of this experiment. First, if a number of isomers lie so close together in energy, how is it that only one of them seems to be observed? One possibility might be that the other isomers are also present in the beam, but do not have a spectral feature in the range scanned experimentally. In fact, simulations reveal numerous isomers of all three morphologies illustrated in Fig. 5 with different arrangements of the hydrogen bonds. The remaining discussion will concentrate on the cage and the results of calculations using the ASP-W2 and TIP4P potentials described in §3. The ASP-W2 form should be very similar to that employed in the DMC calculations of nuclear dynamics by Liu *et al.* [82]. However, we note that the cage isomer is also not the lowest in energy for either of these potentials, although

Fig. 5. Cage, prism and book forms of $(\text{H}_2\text{O})_6$.

inclusion of zero-point energy can alter the ordering [82]. In fact, for the ASP-W2 potential the cyclic structure of the water pentamer is also not the global minimum, but nevertheless, the lowest energy rearrangements of this isomer are quite well reproduced [46].

For the ASP-W2 potential only the first order induction energy was considered, since iterating this term to convergence is time-consuming and was found to make no qualitative difference to results for the water pentamer in previous work [46]. There are then four isomers of the cage structure shown in Fig. 5 differing only in the position of the free hydrogen atoms of the two terminal, single-donor, single-acceptor monomers (Fig. 6). No low energy degenerate rearrangements of these isomers were found, but transition states were located for non-degenerate single flip and bifurcation mechanisms. For every single flip process there is an analogous bifurcation which links different permutational isomers of the same structures. Details of the paths are given in Table 3 and the single flip and bifurcation pathways linking cage isomers C1 and C2 are illustrated in Fig. 7 and Fig. 8. The other paths are omitted for brevity.

The experimental VRT transition has been assigned to a torsional motion of one of the single-donor, single-acceptor monomers, and the form of the spectrum has been described as ‘near-prolate’ [82]. Note that even with full vibrational averaging over the four cage isomers in Fig. 6 a symmetric top spectrum would not be expected. Experimentally, every line was found to be split into a triplet with intensities in the ratio 9:6:1 and equal spacings of 1.92 MHz [82]. Liu *et al.* have explained how this pattern might emerge in terms of hypothetical degenerate rearrangements of the cage which they assumed must interchange the hydrogens of two monomers in almost equivalent environments. This could lead to a doublet of doublets where the middle lines are essentially superimposed. The resulting nuclear spin weights can then reproduce the observed intensity pattern [82].

Table 3. Rearrangement mechanisms which interconvert cage isomers of $(\text{H}_2\text{O})_6$ calculated with the ASP-W2 potential. The energies are in cm^{-1} . Min_1 is the lower minimum, Δ_1 is the higher barrier, TS is the transition state and Δ_2 is the smaller barrier corresponding to the higher minimum Min_2 . S is the integrated path length in Å, D is the displacement between minima in Å and γ is the cooperativity index. All these quantities are defined in §3.

Min_1	Δ_1	TS	Δ_2	Min_2	S	D	γ	description
C1	560	-15,428	508	C2	2.8	2.1	13.7	single flip
C1	641	-15,347	589	C2	2.9	2.2	7.6	bifurcation
C1	323	-15,664	251	C3	1.7	1.3	15.4	single flip
C1	1,135	-14,853	1,063	C3	3.2	2.1	8.5	bifurcation
C2	325	-15,612	285	C4	1.7	1.3	16.2	single flip
C2	1,058	-14,878	1,018	C4	3.4	2.1	8.6	bifurcation
C3	524	-15,391	506	C4	2.7	2.0	14.1	single flip
C3	650	-15,266	631	C4	2.7	2.2	7.9	bifurcation

Liu *et al.* additionally suggested that the two monomers in question might be the two terminal molecules which we have found to undergo flip and bifurcation rearrangements above. However, no direct degenerate rearrangements of the cage isomers have been found to date. Since a combination of sequential bifurcation and flip rearrangements would achieve the desired effect we will now consider the splittings that might result in more detail. The eight single flip and bifurcation processes described above for the cage isomers link 16 versions: four of each isomer. To distinguish between versions of each isomer we need only specify which of the two hydrogens is free, and so we label the hydrogens on the terminal monomer with two double-acceptor neighbours a and b and those on the monomer with two double-donor neighbours c and d. The four relevant versions of the C1 isomer may then be written C1(ac), C1(bc), C1(ad) and C1(bd). The interconnectivity of all 16 versions is shown in Fig. 9. If we make a Hückel-type approximation then the resulting secular determinant is:

Fig. 6. Isomers of the cage structure for $(\text{H}_2\text{O})_6$ calculated using the ASP-W2 potential with binding energies in cm^{-1} .

Fig. 7. Single flip mechanism which interconverts C1 and C2 for the ASP-W2 potential.

Fig. 8. Bifurcation mechanism which interconverts C1 and C2 for the ASP-W2 potential.

$$\begin{pmatrix}
0 & 0 & 0 & 0 & f_{12} & b_{12} & 0 & 0 & f_{13} & 0 & b_{13} & 0 & 0 & 0 & 0 & 0 \\
0 & 0 & 0 & 0 & b_{12} & f_{12} & 0 & 0 & 0 & f_{13} & 0 & b_{13} & 0 & 0 & 0 & 0 \\
0 & 0 & 0 & 0 & 0 & 0 & f_{12} & b_{12} & b_{13} & 0 & f_{13} & 0 & 0 & 0 & 0 & 0 \\
0 & 0 & 0 & 0 & 0 & 0 & 0 & 0 & b_{13} & 0 & f_{13} & 0 & 0 & 0 & 0 & 0 \\
f_{12} & b_{12} & 0 & 0 & 52 & 0 & 0 & 0 & 0 & 0 & 0 & 0 & f_{24} & 0 & b_{24} & 0 \\
b_{12} & f_{12} & 0 & 0 & 0 & 52 & 0 & 0 & 0 & 0 & 0 & 0 & 0 & f_{24} & 0 & b_{24} \\
0 & 0 & f_{12} & b_{12} & 0 & 0 & 52 & 0 & 0 & 0 & 0 & 0 & b_{24} & 0 & f_{24} & 0 \\
0 & 0 & b_{12} & f_{12} & 0 & 0 & 0 & 52 & 0 & 0 & 0 & 0 & 0 & b_{24} & 0 & f_{24} \\
f_{13} & 0 & b_{13} & 0 & 0 & 0 & 0 & 0 & 72 & 0 & 0 & 0 & f_{34} & b_{34} & 0 & 0 \\
0 & f_{13} & 0 & b_{13} & 0 & 0 & 0 & 0 & 0 & 72 & 0 & 0 & b_{34} & f_{34} & 0 & 0 \\
b_{13} & 0 & f_{13} & 0 & 0 & 0 & 0 & 0 & 0 & 0 & 72 & 0 & 0 & 0 & f_{34} & b_{34} \\
0 & b_{13} & 0 & f_{13} & 0 & 0 & 0 & 0 & 0 & 0 & 0 & 72 & 0 & 0 & b_{34} & f_{34} \\
f_{24} & 0 & b_{24} & 0 & f_{24} & 0 & b_{24} & 0 & f_{34} & b_{34} & 0 & 0 & 91 & 0 & 0 & 0 \\
0 & f_{24} & 0 & b_{24} & 0 & f_{24} & 0 & b_{24} & b_{34} & f_{34} & 0 & 0 & 0 & 91 & 0 & 0 \\
b_{24} & 0 & f_{24} & 0 & b_{24} & 0 & f_{24} & 0 & 0 & 0 & f_{34} & b_{34} & 0 & 0 & 91 & 0 \\
0 & b_{24} & 0 & f_{24} & 0 & b_{24} & 0 & f_{24} & 0 & 0 & b_{34} & f_{34} & 0 & 0 & 0 & 91
\end{pmatrix}$$

where f_{ij} and b_{ij} are the appropriate tunneling matrix elements between C_i and C_j . We can simplify this problem by focusing on one of the isomers, say C_1 , and considering an effective generator [85] corresponding to a flip and a bifurcation (in either order). The reaction graph can then be represented as shown in Fig. 10, where the double lines indicate that there are two routes between each pair of versions depending upon whether the flip or bifurcation comes first. The effective MS group contains the elements E , (ab), (bc) and (ab)(bc) and is isomorphic to C_{2v} . If the four connections are each represented by the same tunneling matrix element β then the energy level pattern will be identical to that obtained in the Hückel treatment of the π system of butadiene, i.e.

$$2\beta(A_1), \quad 0(A_2, B_1), \quad -2\beta(B_2), \quad (5)$$

where the correspondence between the MS group elements and the operations of C_{2v} has been chosen as (cd) $\equiv C_2$, (ab) $\equiv \sigma_v(xz)$ and (ab)(cd) $\equiv \sigma'_v(yz)$. The accidental degeneracy of the A_2 and B_1 states would be broken at higher resolution. The relative nuclear spin weights for rovibronic states are easily shown to be 9:3:3:1 for $(\text{H}_2\text{O})_6$ and 4:2:2:1 for $(\text{D}_2\text{O})_6$ corresponding to $A_1:A_2:B_1:B_2$. If the accidental degeneracy is unresolved then the relative intensities of the three triplet components would be 9:6:1 for $(\text{H}_2\text{O})_6$ and 4:4:1 for $(\text{D}_2\text{O})_6$.

The above analysis leads to the same result as that obtained by Liu *et al.* [82], who considered the consequences of hypothetical direct permutations (ab) and (cd). However, in the present picture the tunneling between different versions of the four cage isomers does not occur through a single barrier, which might explain why the splittings are rather small. For this framework to be consistent we would expect to find similar splitting patterns for all four cage isomers, although the magnitude of the splitting could be different for each one.

The same analysis would also hold for a second family of cage isomers where the double acceptor monomers are adjacent. However, the four corresponding isomers in this case lie several hundred wavenumbers higher in energy than

Fig. 9. Connectivity of versions of the cage isomers C1, C2, C3 and C4 according to the rearrangements listed in Table 3. Solid lines represent the four single flip processes and dashed lines the four bifurcations.

those considered above. Several mechanisms interconverting the two cage families were found in the set of 900 pathways calculated for the hexamer in this study. One further point worthy of consideration is that the experiment measures the difference in tunneling splittings between different rovibrational states. If the observed vibrational transition does indeed correspond to the torsional motion of a single-donor, single-acceptor monomer then the splitting in the excited state could be significantly different from the ground state.

For the TIP4P potential the situation is slightly different because there are only two cage isomers rather than four. The single-donor, single-acceptor that has two double-donor neighbours exhibits only one torsional minimum intermediate between the two states found in C1-C4 above. The other single-donor, single-acceptor has the same two torsional states as in C1-C4, and undergoes single flip

Fig. 10. Effective reaction graph for the four versions of cage isomer C1 that are interconnected indirectly by flip and bifurcation rearrangements.

and bifurcation rearrangements as before. For the single-donor, single-acceptor monomer in the intermediate torsional state a direct degenerate rearrangement corresponding to a bifurcated transition state was found. The pathways are summarized in Table 4 where we label the two isomers C1' and C2'. Illustrations of these rearrangements are omitted for brevity. A degenerate bifurcation rearrangement of the C2' isomer could not be located, despite starting a number of transition state searches from points around the expected geometry.

Table 4. Rearrangement mechanisms which interconvert cage isomers of $(\text{H}_2\text{O})_6$ calculated with the TIP4P potential. The energies are in cm^{-1} . Min_1 is the lower minimum, Δ_1 is the higher barrier, TS is the transition state, and Δ_2 is the smaller barrier corresponding to the higher minimum Min_2 . S is the integrated path length in Å , D is the displacement between minima in Å and γ is the cooperativity index. All these quantities are defined in §3.

Min_1	Δ_1	TS	Δ_2	Min_2	S	D	γ	description
C1' (-16,533)	14	-16,519	2	C2' (-16,521)	1.3	1.2	14.1	single flip
C1' (-16,533)	825	-15,708	813	C2' (-16,521)	3.6	2.2	8.6	bifurcation
C1' (-16,533)	1,361	-15,172	1,361	C1' (-16,533)	4.5	2.2	8.7	bifurcation

Although the topology of the PES is different for the TIP4P potential the above rearrangements could produce the same tunneling splittings and intensity pattern as before, since there are still pathways linking all four versions of each isomer. Unfortunately there is insufficient experimental information to distinguish the two possibilities, and it is quite possible that neither scenario is correct.

Due to the relatively large number of degrees of freedom and the uncertainties associated with the choice of empirical potential more accurate theoretical treatments of the dynamics will not be easy. However, it may not be a bad approximation to neglect relaxations of the rest of the cage in considering the dynamics of the two single-donor, single-acceptor monomers. Two-dimensional quantum calculations of the torsional dynamics of these two molecules were performed under this approximation using the C1 geometry and the discrete variable representation [86] (DVR). These calculations follow the three-dimensional DVR calculations of Sabo *et al.* [29] for (H₂O)₃ in employing a model Hamiltonian in which only rotation about the hydrogen-bonded O–H bond is permitted:

$$\hat{\mathcal{H}} = -B_{\text{eff}} \left(\frac{\partial^2}{\partial \phi_1^2} + \frac{\partial^2}{\partial \phi_2^2} \right) + V(\phi_1, \phi_2), \quad (6)$$

where ϕ_1 and ϕ_2 are the two torsional angles in question and the value of B_{eff} was taken to be 19.63 cm⁻¹ for H₂O and 9.82 cm⁻¹ for D₂O. For each torsional degree of freedom the basis functions were chosen as:

$$\psi(\phi) = \frac{1}{\sqrt{2\pi}} e^{im\phi}, \quad m = 0, \pm 1, \dots, \pm N, \quad (7)$$

giving a total of $(2N + 1)^2$ basis functions for a given value of N . The DVR grid points are then uniformly spaced in each coordinate:

$$\phi^j = \frac{2\pi j}{2N + 1}, \quad j = 1, 2, \dots, 2N + 1. \quad (8)$$

Hence we obtain a direct product DVR with grid points (ϕ_1^j, ϕ_2^k) , and using the known analytic form for the kinetic energy operator [87] we obtain the Hamiltonian matrix elements:

$$H_{cd}^{ab} = T_{ca} \delta_{db} + T_{db} \delta_{ca} + V(\phi_1^c, \phi_2^d) \delta_{ac} \delta_{db}, \quad (9)$$

where

$$T_{ca} = B_{\text{eff}} (-1)^{c-a} \begin{cases} N(N + 1)/3, & a = c, \\ \frac{\cos[\pi(c - a)/(2N + 1)]}{2 \sin^2[\pi(c - a)/(2N + 1)]}, & a \neq c. \end{cases} \quad (10)$$

The lowest eigenvalues were converged to an accuracy better than 0.1 cm⁻¹ for both (H₂O)₆ and (D₂O)₆ at a value $N = 14$; an iterative Lanczos matrix diagonalization procedure was employed.

The lowest eight eigenvectors for (H₂O)₆ along with assignments are shown in Fig. 11 for ASP-W2 and Fig. 12 for TIP4P. In both cases the ranges of the torsional angles have been restricted to exclude regions where the amplitude is essentially always zero. The centre of each surface corresponds to the geometry with both free hydrogens in intermediate positions. Not surprisingly, the wavefunctions for the TIP4P potential are all delocalized over torsional space, and can be classified according to the number of nodes in the ϕ_1 and ϕ_2 directions. The three lowest energy wavefunctions for the ASP-W2 potential are localized

Fig. 11. Amplitudes of the lowest eight eigenvectors in torsional space found by two-dimensional DVR calculations for $(\text{H}_2\text{O})_6$ with the ASP-W2 potential. The interval between grid lines is 12.41° in both directions.

in the wells corresponding to C1, C2 and C3. However, the fourth, seventh and eighth functions appear to be delocalized over two isomers in each case. For this potential the wavefunctions are described in terms of localized functions in the four different wells, e.g. C1(1,0) is the function localized in the C1 well with one node in the ϕ_1 direction and none in the ϕ_2 direction. The results for $(D_2O)_2$ are omitted for brevity, and can be obtained from the author on request.

Clearly we cannot assign the experimental transition on the basis of these model calculations. However, the fact that both potentials exhibit some delocalization between different cage isomers suggests that vibrational averaging of the structure is likely, especially in an excited torsional state. Unfortunately, it does not seem to be possible to admit both the flip and bifurcation rearrangements without including at least three angular degrees of freedom for each of the two monomers in question. Such calculations are considerably more difficult, and are left for future work.

References

1. D. D. Nelson, G. T. Fraser and W. Klemperer, *Science* **238**, 1670 (1987).
2. G. C. Maitland, M. Rigby, E. B. Smith and W. A. Wakeham, *Intermolecular Forces* (Clarendon Press; Oxford, 1981).
3. R. C. Cohen and R. J. Saykally, *Annu. Rev. Phys. Chem.* **42**, 369 (1991).
4. J. M. Hutson, *Annu. Rev. Phys. Chem.* **41**, 123 (1990).
5. R. C. Cohen and R. J. Saykally, *J. Phys. Chem.* **94**, 7991 (1990).
6. N. Pugliano and R. J. Saykally, *J. Chem. Phys.* **96**, 1832 (1992).
7. R. J. Saykally and G. A. Blake, *Science* **259**, 1570 (1993).
8. K. Liu, J. D. Cruzan and R. J. Saykally, *Science* **271**, 929 (1996).
9. N. Pugliano and R. J. Saykally, *Science* **257**, 1937 (1992).
10. J. Del Bene and J. A. Pople, *J. Chem. Phys.* **58**, 3605 (1973).
11. M. F. Vernon, D. J. Krajnovich, H. S. Kwok, J. M. Lisy, Y. R. Shen and Y. T. Lee, *J. Chem. Phys.* **77**, 47 (1982).
12. Owicki, J. C.; Shipman, L. L.; Scheraga, H. A., *J. Phys. Chem.* **79**, 1794 (1975).
13. D. J. Wales, *J. Amer. Chem. Soc.* **115**, 11180 (1993).
14. J. E. Fowler and H. F. Schaefer, *J. Amer. Chem. Soc.* **117**, 446 (1995).
15. K. Liu, J. G. Loeser, M. J. Elrod, B. C. Host, J. A. Rzepiela, N. Pugliano and R. J. Saykally, *J. Amer. Chem. Soc.* **116**, 3507 (1994).
16. S. Suzuki and G. A. Blake, *Chem. Phys. Lett.* **229**, 499 (1994).
17. T. R. Walsh and D. J. Wales, *J. Chem. Soc., Faraday Trans.* **92**, 2505 (1996).
18. J. G. C. M. van Duijneveldt-van de Rijdt and F. B. van Duijneveldt, *J. Chem. Phys.* **97**, 5019 (1982).
19. G. Chalasiński, M. M. Szczeniński, P. Cieplak and S. Scheiner, *J. Chem. Phys.* **94**, 2873 (1991).
20. S. S. Xantheas and T. H. Dunning, *J. Chem. Phys.* **98**, 8037 (1993).
21. S. S. Xantheas and T. H. Dunning, *J. Chem. Phys.* **99**, 8774 (1993).
22. S. S. Xantheas, *J. Chem. Phys.* **100**, 7523 (1994).

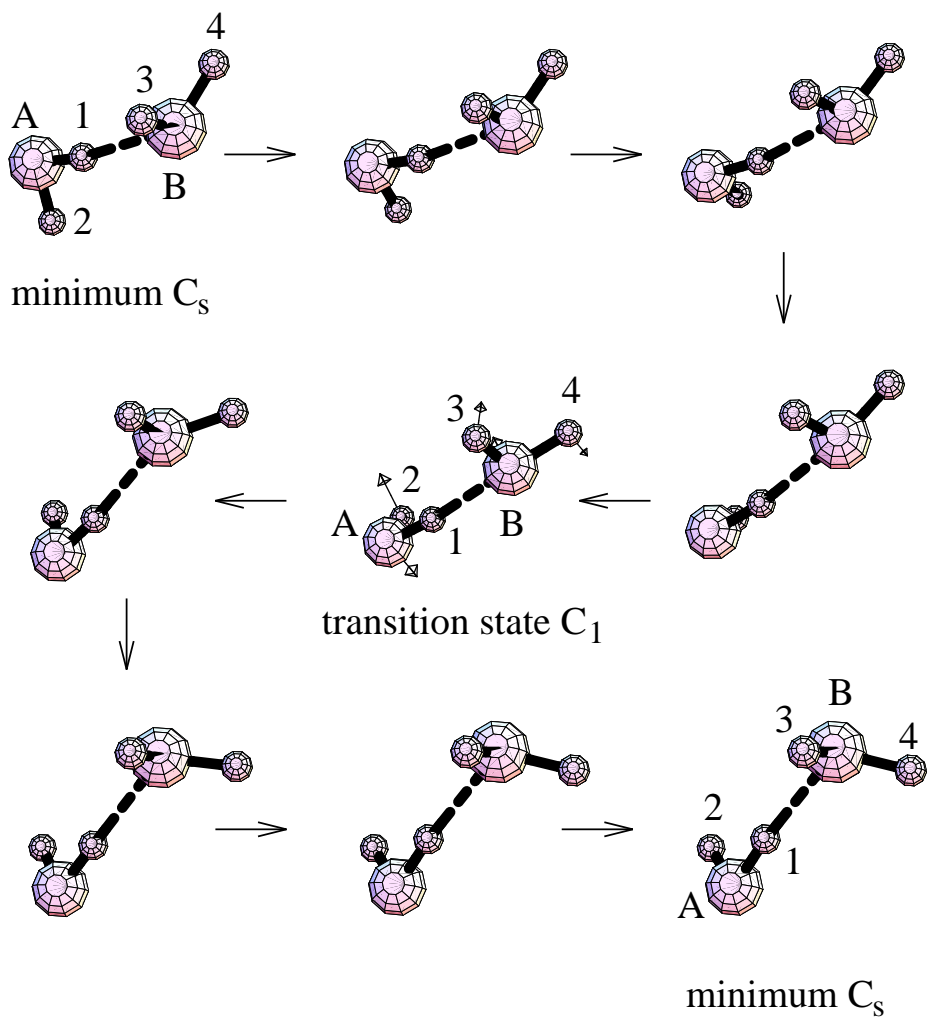
Fig. 12. Amplitudes of the lowest eight eigenvectors in torsional space found by two-dimensional DVR calculations for $(\text{H}_2\text{O})_6$ with the TIP4P potential. The interval between grid lines is 12.41° in both directions.

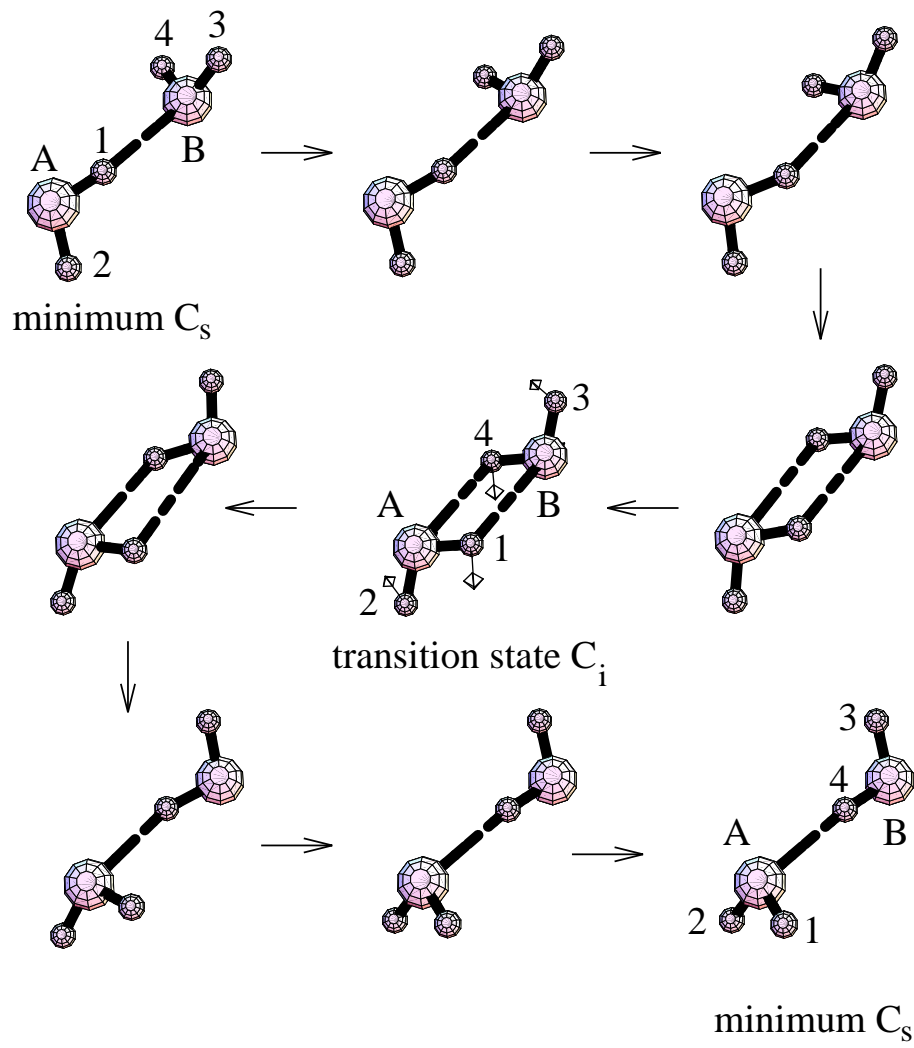
23. van Duijneveldt-van de Rijdt, J. G. C. M.; van Duijneveldt, F. B., *Chem. Phys. Lett.* **237**, 560-567 (1995).
24. W. Klopper, M. Schütz, H. P. Lüthi and Leutwyler, S., *J. Chem. Phys.* **103**, 1085 (1995).
25. T. Bürgi, S. Graf, S. Leutwyler and W. Klopper, *J. Chem. Phys.* **103**, 1077 (1995).
26. M. Schütz, T. Bürgi, S. Leutwyler and H. B. Bürgi, *J. Chem. Phys.* **99**, 5228 (1993).
27. M. Schütz, T. Bürgi, S. Leutwyler and H. B. Bürgi, *J. Chem. Phys.* **100**, 1780 (1994).
28. W. Klopper and M. Schütz, *Chem. Phys. Lett.* **237**, 536 (1995).
29. D. Sabo, Z. Bačić, T. Bürgi and S. Leutwyler, *Chem. Phys. Lett.* **244**, 283 (1995).
30. J. K. Gregory and D. C. Clary, *J. Chem. Phys.* **102**, 7817 (1995).
31. J. K. Gregory and D. C. Clary, *J. Chem. Phys.* **103**, 8924 (1995).
32. R. G. A. Bone, T. W. Rowlands, N. C. Handy and A. J. Stone, *Molec. Phys.* **72**, 33-73 (1991).
33. D. M. Dennison and J. D. Hardy, *Phys. Rev.* **39**, 938-947 (1932).
34. R. P. Bell, *The Tunnel Effect in Chemistry* (Chapman and Hall; New York, 1980).
35. R. E. Leone and P. v. R. Schleyer, *Angew. Chem. Int. Ed. Engl.* **9**, 860 (1970).
36. J. G. Nourse, *J. Amer. Chem. Soc.* **102**, 4883 (1980).
37. J. N. Murrell and K. J. Laidler, *J. Chem. Soc., Faraday II* **64**, 371 (1968).
38. H. C. Longuet-Higgins, *Molec. Phys.* **6**, 445 (1963).
39. J. T. Hougen, *J. Chem. Phys.* **37**, 1433 (1962).
40. J. T. Hougen, *J. Chem. Phys.* **39**, 358 (1962).
41. J. T. Hougen, *J. Phys. Chem.* **90**, 562 (1986).
42. P. R. Bunker, *Molecular Symmetry and Spectroscopy* (Academic Press; New York, 1970).
43. D. J. Wales, *J. Amer. Chem. Soc.* **115**, 11191 (1993).
44. C. J. Cerjan and W. H. Miller, *J. Chem. Phys.* **75**, 2800 (1981); J. Simons, P. Jørgenson, H. Taylor and J. Ozment, *J. Phys. Chem.* **87**, 2745 (1983); D. O'Neal, H. Taylor and J. Simons, *J. Phys. Chem.* **88**, 1510 (1984); A. Banerjee, N. Adams, J. Simons and R. Shepard, *J. Phys. Chem.* **89**, 52 (1985); J. Baker, *J. Comput. Chem.* **7**, 385 (1986); J. Baker, *J. Comput. Chem.* **8**, 563 (1987).
45. D. J. Wales, *J. Chem. Phys.* **101**, 3750 (1994).
46. D. J. Wales and T. R. Walsh, *J. Chem. Phys.* **105**, 6957 (1996).
47. R. D. Amos and J. E. Rice, *CADPAC: the Cambridge Analytic Derivatives Package, Issue 4.0*; Cambridge, 1987.
48. A. Banerjee and N. P. Adams, *Int. J. Quant. Chem.* **43**, 855 (1992).
49. P. L. A. Popelier, A. J. Stone and D. J. Wales, *J. Chem. Soc., Faraday Discuss.* **97**, 243 (1994).
50. D. J. Wales, P. L. A. Popelier and A. J. Stone, *J. Chem. Phys.* **102**, 5556 (1995).

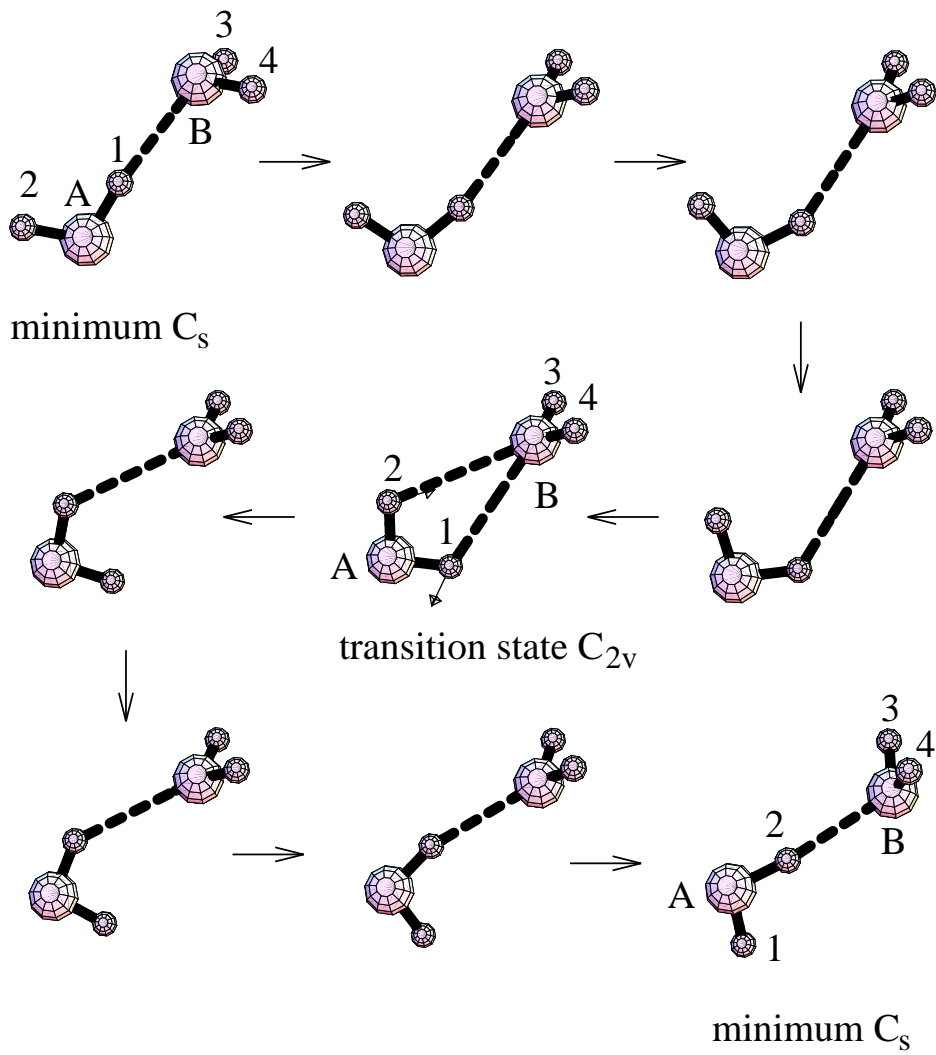
51. D. J. Wales, A. J. Stone and P. L. A. Popelier, Chem. Phys. Lett. **240**, 89 (1995).
52. A. J. Stone, Chem. Phys. Lett. **83**, 233 (1981).
53. A. J. Stone and M. Alderton, Molec. Phys. **56**, 1047 (1985).
54. A. J. Stone, Molec. Phys. **56**, 1065 (1985).
55. C. R. Le Sueur and A. J. Stone, Molec. Phys. **78**, 1267 (1993).
56. C. Millot and A. J. Stone, Molec. Phys. **77**, 439 (1992).
57. W. L. Jorgensen, J. Amer. Chem. Soc. **103**, 335 (1981).
58. W. L. Jorgensen, J. Chandraesekhar, J. W. Madura, R. W. Impey and M. L. Klein, J. Chem. Phys. **79**, 926 (1983).
59. T. H. Dunning Jr., J. Chem. Phys. **53**, 2823 (1970).
60. S. J. Huzinaga, J. Chem. Phys. **47**, 1293 (1965).
61. C. Møller and M. S. Plesset, Phys. Rev. **46**, 618 (1934).
62. A. D. Becke, Phys. Rev. A **38**, 3098 (1988).
63. C. Lee, W. Yang and R. G. Parr, Phys. Rev. B **37**, 785 (1988).
64. F. H. Stillinger and T. A. Weber, Phys. Rev. A **28**, 2408 (1983).
65. G. T. Fraser, Int. Rev. Phys. Chem. **10**, 189 (1991).
66. T. R. Dyke, K. M. Mack and J. S. Muentner, J. Chem. Phys. **66**, 498 (1977).
67. N. Pugliano, J. D. Cruzan, J. G. Loeser and R. J. Saykally, J. Chem. Phys. **98**, 6600 (1993).
68. T. R. Dyke, J. Chem. Phys. **66**, 492 (1977).
69. J. T. Hougen, J. Mol. Spectr. **114**, 395 (1985).
70. L. H. Coudert and J. T. Hougen, J. Mol. Spectr. **130**, 86 (1988).
71. L. H. Coudert and J. T. Hougen, J. Mol. Spectr. **139**, 259 (1990).
72. B. J. Smith, D. J. Swanton, J. A. Pople, H. F. Schaefer and L. Radom, J. Chem. Phys. **92**, 1240 (1990).
73. S. F. Boys and F. Bernardi, Molec. Phys. **19**, 553 (1970).
74. S. S. Xantheas, J. Chem. Phys. **104**, 8821 (1996).
75. J. A. Odutola and T. R. Dyke, J. Chem. Phys. **72**, 5062 (1980).
76. M. Tsuboi, A. Y. Hirakawa, T. Ino, T. Sasaki and K. Tamagake, J. Chem. Phys. **41**, 2721 (1964).
77. Mathematica 2.0; Wolfram Research Inc., Champaign, IL, 1989.
78. E. Zwart, J. J. ter Muelen, W. L. Meerts and L. H. Coudert, J. Mol. Spectrosc. **147**, 27 (1991).
79. S. C. Althorpe and D. C. Clary, J. Chem. Phys. **101**, 3603 (1995).
80. D. J. Wales, J. Amer. Chem. Soc. **115**, 11191 (1993).
81. C. A. Coulson and S. Rushbrooke, Proc. Camb. Phil. Soc. **36**, 193 (1940).
82. K. Liu, M. G. Brown, C. Carter, R. J. Saykally, J. K. Gregory and D. C. Clary, Nature **381**, 501 (1996).
83. C. J. Tsai and K. D. Jordan, Chem. Phys. Lett. **213**, 181-188 (1993).
84. K. Kim, K. D. Jordan and T. S. Zwier, J. Amer. Chem. Soc. **116**, 11568-11569 (1994).
85. B. J. Dalton and P. D. Nicholson, Int. J. Quantum Chem. **9**, 325 (1975).
86. Z. Bačić and J. C. Light, Annu. Rev. Phys. Chem. **40**, 469 (1989).
87. D. T. Colbert and W. H. Miller, J. Chem. Phys. **96**, 1982 (1992).

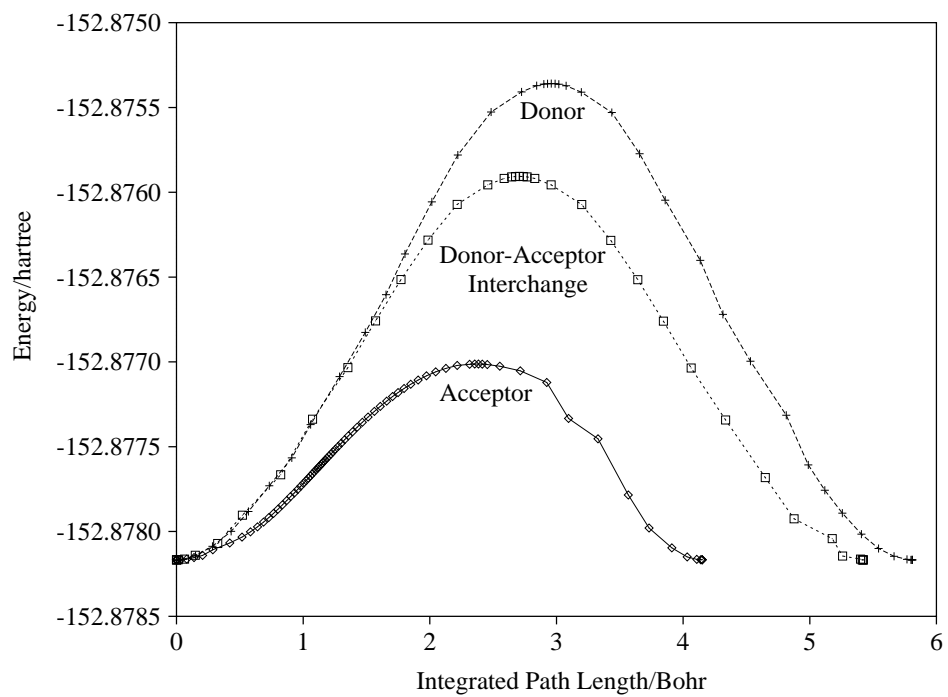
Since this paper was written in October 1996 a number of additional publications have appeared on the subject of small water clusters. The most relevant are collected here for convenience.

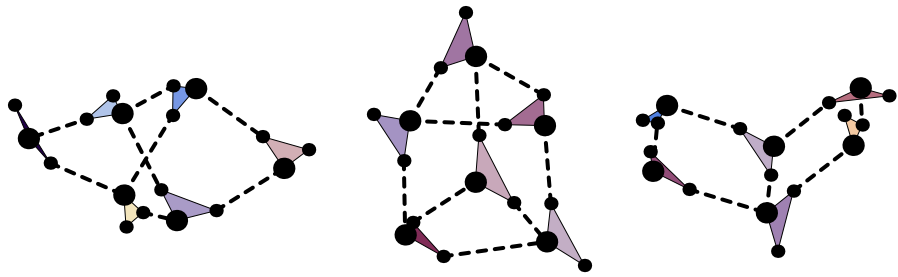
- (a) J. K. Gregory, *Chem. Phys. Lett.* **282**, 147 (1998).
- (b) C. S. Guiang and R. E. Wyatt, *Int. J. Quantum Chem.* **68**, 233 (1998).
- (c) I. M. Quintana, W. Ortiz and G. E. Lopez, *Chem. Phys. Lett.* **287**, 429 (1998).
- (d) J. B. Paul, R. A. Provencal and R. J. Saykally, *J. Phys. Chem. A* **102**, 3279 (1998).
- (e) O. Engkvist, N. Forsberg, M. Schütz and G. Karlstrom, *Molec. Phys.* **90**, 277 (1997).
- (f) J. K. Gregory and D. C. Clary, *J. Phys. Chem. A* **101**, 6813 (1997).
- (g) J. K. Gregory, D. C. Clary, K. Liu, M. G. Brown and R. J. Saykally, *Science* **275**, 814 (1997).
- (h) M. P. Hodges, A. J. Stone and S. S. Xantheas, *J. Phys. Chem. A* **101**, 9163 (1997).
- (i) C. Leforestier, L. B. Braly, K. Liu, M. J. Elrod and R. J. Saykally, *J. Chem. Phys.* **106**, 8527 (1997).
- (j) M. Schütz, S. Brdarski, P.-O. Widmark, R. Lindh and G. Karlström, *J. Chem. Phys.* **107**, 4597 (1997).
- (k) J. B. Paul, C. P. Collier, R. J. Saykally, J. J. Scherer and A. O'Keefe, *J. Phys. Chem. A* **101**, 5211 (1997).
- (l) M. R. Viant, J. D. Cruzan, D. D. Lucas, M. G. Brown, K. Liu and R. J. Saykally, *J. Phys. Chem. A* **101**, 9032 (1997).
- (m) J. D. Cruzan, M. R. Viant, M. G. Brown and R. J. Saykally, *J. Phys. Chem. A* **101**, 9022 (1997).
- (n) K. Liu, M. G. Brown and R. J. Saykally, *J. Phys. Chem. A* **101**, 8995 (1997).
- (o) J. D. Cruzan, L. B. Braly, K. Liu, M. G. Brown, J. G. Loeser and R. J. Saykally, *Science* **271**, 59 (1996).
- (p) E. Fredj, R. B. Gerber and M. A. Ratner, *J. Chem. Phys.* **105**, 1121 (1996).
- (q) J. K. Gregory and D. C. Clary, *J. Phys. Chem.* **100**, 18014 (1996).
- (r) K. Liu, M. G. Brown, J. D. Cruzan and R. J. Saykally, *Science* **271**, 62 (1996).
- (s) K. Liu, M. G. Brown, M. R. Viantm, J. D. Cruzan and R. J. Saykally, *Mol. Phys.* **89**, 1373 (1996).
- (t) E. M. Mas and K. Szalewicz, *J. Chem. Phys.* **104**, 7606 (1996).
- (u) E. H. T. Olthof, A. Van der Avoird, P. E. S. Wormer, K. Liu and R. J. Saykally, *J. Chem. Phys.* **105**, 8051 (1996).
- (v) J. M. Pedulla, F. Vila and K. D. Jordan, *J. Chem. Phys.* **105**, 11091 (1996).
- (w) D. Sabo, Z. Bačić, T. Bürgi and S. Leutwyler, *Chem. Phys. Lett.* **261**, 318 (1996).
- (x) J. M. Sorenson, J. K. Gregory and D. C. Clary, *Chem. Phys. Lett.* **263**, 680 (1996).
- (y) A. Van der Avoird, E. H. T. Olthof and P. E. S. Wormer, *J. Chem. Phys.* **105**, 8034 (1996).

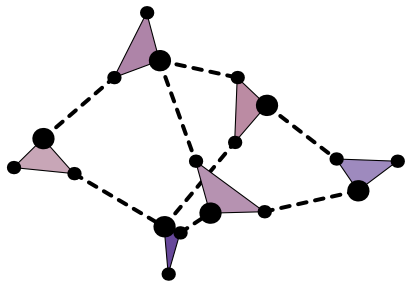




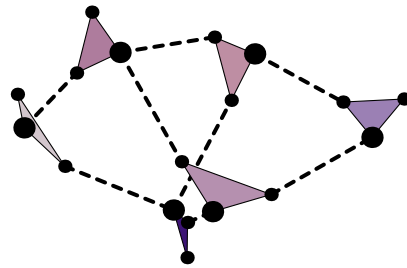




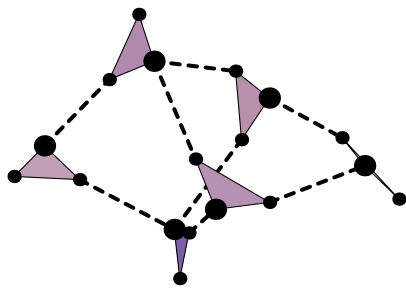




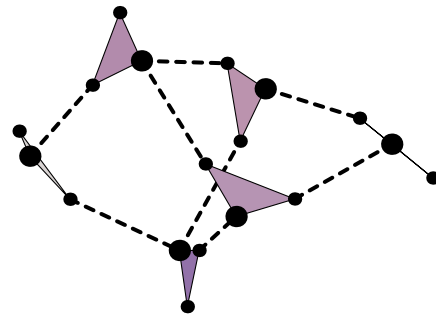
C1 -15,988



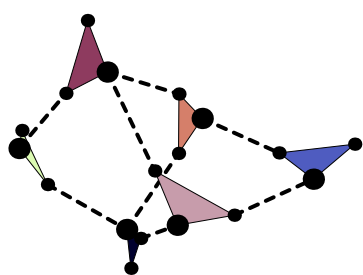
C2 -15,936



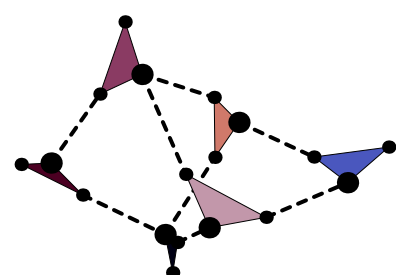
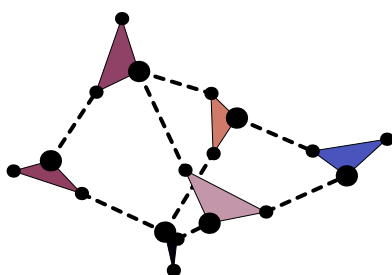
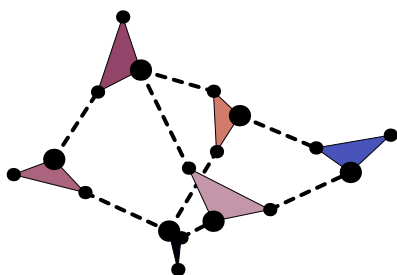
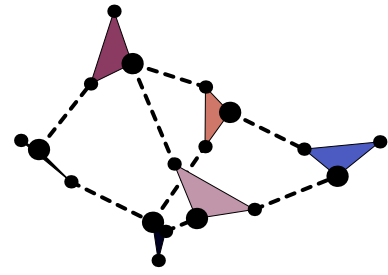
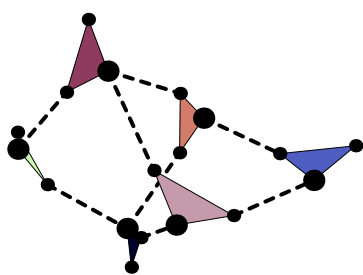
C3 -15,916



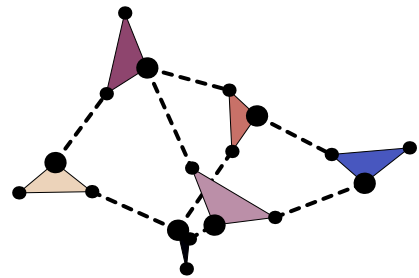
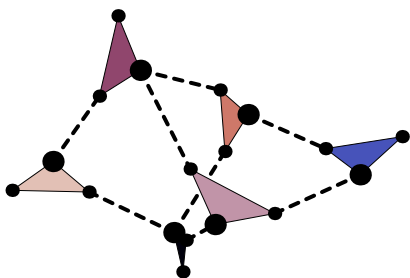
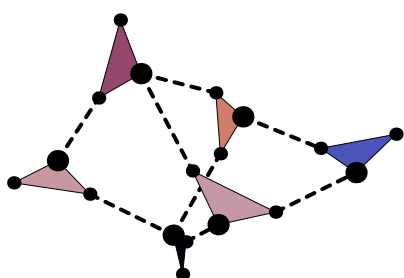
C4 -15,897



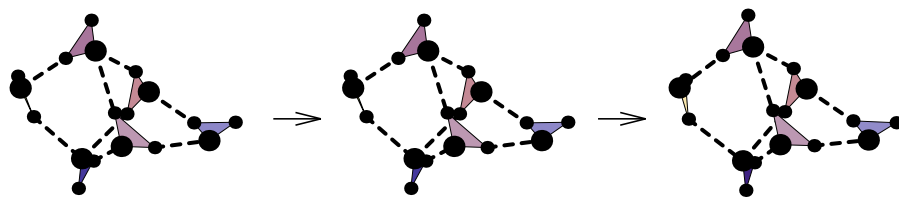
minimum C2



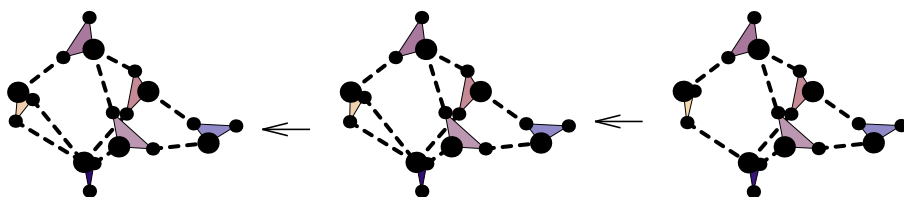
transition state



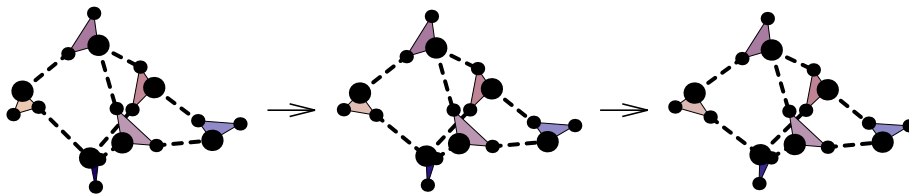
minimum C1



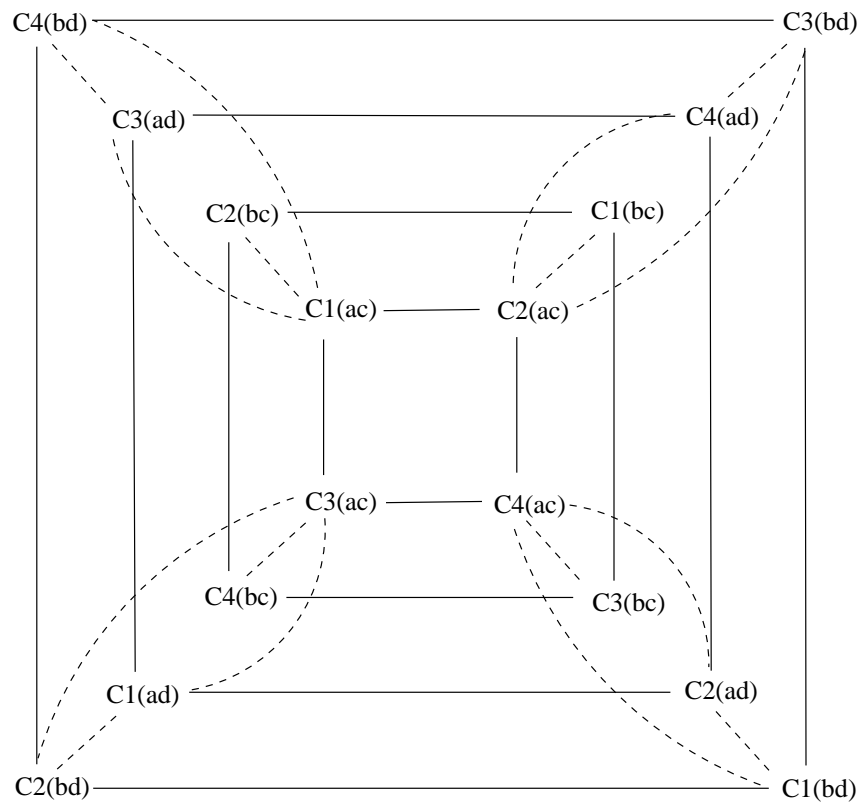
minimum C2



transition state



minimum C1



$$\begin{array}{ccc}
\text{C1(ac)} & \text{-----} & \text{C1(bc)} \\
\left| \right. & & \left. \right| \\
& f_{12} + b_{12} & \\
f_{13} + b_{13} & & f_{24} + b_{24} \\
& f_{34} + b_{34} & \\
\left| \right. & \text{-----} & \left. \right| \\
\text{C1(ad)} & & \text{C1(bd)}
\end{array}$$

